

Low-Dose CT Dental Image Denoising by Morphological Operators and 3D Filtering

Romulo Marconato Stringhini, Daniel Welfer
and Marcos Cordeiro d'Ornellas
Department of Applied Computing
Federal University of Santa Maria
Santa Maria, Brazil
Email: [rstringhini,welfer,ornellas]@inf.ufsm.br

Daniel Fernando Tello Gamarra
Department of Electrical Energy Processing
Federal University of Santa Maria
Santa Maria, Brazil
Email: fernandotg99@gmail.com

Abstract—The impact in reducing the radiation dose in computed tomography (CT) exams is directly related to the quality of the images obtained in these exams. Such images are degraded by undesirable artifacts, known as noise. In order to improve the quality of these images and provide an accurate medical diagnosis, it is necessary to apply noise reduction techniques. In this study, a method based on structural segmentation and filtering through morphological operators along with a BM3D filtering is proposed to reduce noise and preserve details in low-dose CT dental images. Experimental results of the proposed method were compared with several existing methods and validated using the PSNR, SSIM, MSE and EPI metrics. Our method demonstrated superior performance among the evaluated filters. In comparison to the filter that obtained the best results, our method had a gain of 12.46% on PSNR, 11.11% on SSIM, 14.5% on MSE and 9.63% on EPI metrics.

I. INTRODUCTION

In the field of medical imaging, computed tomography (CT) is an extremely important tool that examines internal structures of a patient and provides accurate medical diagnosis. In this exam, the dose of radiation is directly associated with the quality of the image acquired. That is, a high radiation dose provides a high quality image. However, exposing patients to high doses of radiation is detrimental to their health. Therefore, in order to prevent the patient to constant radiation exposures, the medical community has been focusing on reducing the dose of radiation applied in CT scans.

Currently, the ALARA (As Low As Reasonably Achievable) principle has been taken as a reference, which aims to minimize the dose of radiation at a "as low as reasonably possible" level, while maintaining an acceptable diagnostic accuracy [1]. Images acquired in low-radiation CT scans are usually impaired by noise, where important structures and details are affected, resulting in poor quality images, which may influence the final medical diagnosis.

Several filters have been proposed in the literature with the purpose of reducing noise and preserving the integrity of important details of the images. A widely used noise filtering technique is the median filter [2]. This filter attempts to restore the intensity value of the corrupted pixel by calculating the median values of the intensities of the neighboring pixels. However, this type of filtering not only reduces present noise

but also damages structural details [3]. Another well-known and used technique is the Gaussian filtering. When applied with optimal parameters, it can be efficient in terms of noise reduction, however, it tends to erase edges and details and can lead to ghost edges [4].

Proposed by Tomasi et al. [5], the bilateral filter smooths the noise and preserves the structural edges of the images. In this method, each pixel is replaced by the weighted average of the values of the intensities of its neighboring pixels, through their proximity and similarity [5]. The bitonic filter, proposed by Graham Treece [6], presents better edge preservation and detail than the median filter and greater noise reduction capability than the Gaussian filter. It uses the definition of a signal as being *bitonic*, containing only one local maxima or minima within the filter range [6].

The guided filter [7] can be used as an edge-preserving filter, like the bilateral filter [5] but with better results near edges. The guided filter considers the content of an input image, a guidance image and an output image [7]. A sliding window $M \times N$ processes the pixels of the guidance image and applies the result of this step into the input image. The pixel values are calculated according to their respective colors and spatial similarity. After calculating such values, the output image is obtained.

Based on sparse representation in the transform domain, the Block-Matching 3D (BM3D) technique was proposed by Dabov et al. [8]. This technique reduces the noise by processing similar blocks within the image. It groups these similar 2D blocks into 3D arrays, called groups, and performs a collaborative filtering in such groups: initially, through a 3D transform with a hard threshold and, after, through a collaborative Wiener filter. Finally, the output image is reconstructed using a weighted average aggregation [8]. In addition to these examples, several techniques can be found in the literature, such as wavelet transform filtering, introduced by [9], AWMF (Adaptive Weighted Median Filter) [10], AMF (Adaptive Median Filter), PSMF (Progressive Switching Median Filter) [11], NAFSMF (Noise Adaptive Fuzzy Switching Median Filter) [12], DBUTMF (Decision Based Unsymmetrical Trimmed Median Filter) [13], BPDF (Based on Pixel Density Filter) [14], OCS (Open-Close Sequence) filter [15], among others.

Also, recently, filters based on mathematical morphology operators are being commonly used. In image processing, mathematical morphology is used to identify and extract image information based on shape or contour properties of the image through a structuring element [16] which is used to determine the efficiency of the morphological operator. The fundamental operators of mathematical morphology are dilation, erosion, opening and closing [15]. Such operators are efficient not only for noise reduction but also for structural segmentation, information and details extraction or to compress images.

In this study, a noise reduction method focused on low-dose computed tomography dental images is presented. Our method relies on the use of mathematical morphology and has two main stages: image segmentation and noise filtering. The first stage is responsible for extracting the foreground from the background region of the image while the second stage performs the noise filtering with morphological operators and BM3D. Experimental results demonstrated that the proposed method reduced the noise and preserved edges and details more efficiently than the compared filters. To validate its effectiveness, PSNR, MSE, SSIM and EPI were used as quantitative image quality metrics.

The course of this paper is organized as follows: in Section 2 is presented the materials and the proposed method. Experimental results and validation are presented in Section 3. The results are discussed in Section 4 and the work is summarized and concluded in Section 5.

II. MATERIALS AND METHODOLOGY

The low-dose CT dental images used in this study were taken from an anonymized database from the University Hospital of Santa Maria. These images are contaminated with natural noise acquired during the scanning process. Our proposed noise reduction method is presented in two stages: image segmentation and noise filtering.

A. First Stage: Image Segmentation

Image segmentation is a process in which a given image is divided into regions in order to select which will be processed or analyzed separately [17]. To achieve the best performance in the stage of noise filtering, we divided into two different regions: background and foreground.

Firstly, the gray scale level image, denoted f_2 , is obtained from the input noisy image f_1 (see Fig. 1(a)).

Then, a morphological opening by reconstruction is applied in f_2 . First, the opening removes bright features which sizes are smaller than the structuring element and, after that, the dilation restore the contours of components that have not removed by the opening operator. The output image after this reconstruction is denoted f_3 and is described as

$$f_3 = \bigvee_{n \geq 1} \delta_{f_2}^{(n)}(\gamma_{f_2}). \quad (1)$$

where $\gamma_{f_2}^B = \delta^B(\varepsilon^B(f_2))$ is the opening operator in f_2 with a diamond shaped structuring element B of size 2, and

$(\delta^B(f_2))(x) = \max_{b \in B} f_2(x+b)$ is the dilation operator. The image resulted from this step is illustrated in Fig. 1(b).

As the image structures has high contrast with the background region, Otsu threshold method [18] was applied to detect the ground truth region in f_3 . The resulting image f_4 is illustrated in Fig. 1(c). In order to extract the foreground region from the background, an element-wise multiplication was applied between f_4 and the input image f_2 . Done that, we obtained the noisy foreground region f_5 and the noisy background region f_6 , shown in Fig. 1(d) and Fig. 1(e) respectively. These two noisy regions will be processed in the next stage of the proposed method, named as noise filtering.

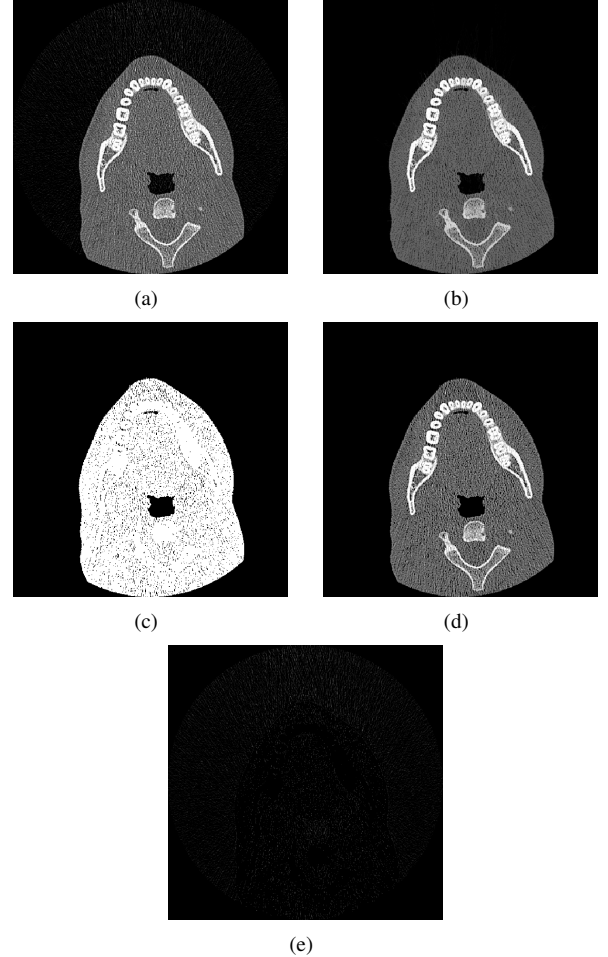


Fig. 1. (a) Gray scale level input image f_2 . (b) Resulting image f_3 from opening by reconstruction. (c) Ground truth image f_4 after Otsu's threshold. (d) Noisy foreground f_5 . (e) Noisy background f_6 .

B. Second Stage: Noise Filtering

The noise filtering stage of our proposed method takes as input images to be processed the noisy foreground region f_5 and the noisy background f_6 . To reduce some of the noisy artifacts present in the foreground region, we firstly applied a morphological opening operator γ in f_5 with the same structuring element B used in the segmentation process,

resulting in the image f_7 illustrated in Fig. 2(a). This operation can be understood as

$$f_7 = \gamma^B = \delta^B(\varepsilon^B(f_5)). \quad (2)$$

This operation removes objects that are smaller than B through the erosion operator and restore in part the remained objects through the morphological dilation.

Before completely restoring the components degraded by the opening operator, we enhanced the preserved details using the CLAHE (Contrast Adaptive Limited Histogram Equalization) enhancement algorithm, obtaining f_8 . CLAHE is an improved version of the adaptive histogram equalization (AHE) [19]. The algorithm basically divides the image into regions of nearly the same size, which will form three different groups. The first group, called corner regions, contains the four corner regions of the image. The second group contains the border regions and is called border group and the rest of the regions are grouped into the internal regions group. After this grouping process, the histogram of each region is enhanced. The regions are combined back to their original positions using bilateral interpolation and the output enhanced image is obtained. In our proposed method, the result of this step can be seen in Fig. 2(b).

Now, to completely restore the components degraded by the morphological opening operator, a morphological reconstruction by dilation was used. In our case, the mask image is the foreground image f_5 and the marker image is the image resulting from CLAHE enhancement f_8 . The resulting reconstructed image f_9 is illustrated in Fig. 2(c) and can be mathematically expressed as

$$f_9 = \bigvee_{n \geq 1} \delta_{f_5}^{(n)}(f_8). \quad (3)$$

However, according to Fig. 2(c), it is possible to notice that noisy artifacts are still present in the foreground region. In order to smooth out the noise, we introduced the Block-Matching 3D (BM3D) filtering technique.

Proposed by Dabov et al. [8], the BM3D is an image denoising technique based on an enhanced sparse representation in the transform domain. The filter can be understood in two steps: basic estimate and final estimate.

In the first step, the filter processes the noisy image f_9 to find similar blocks, grouping them in a 3D array, called groups. Then, it applies a 3D transform and its inverse to each formed group in order to reduce the noise and produce estimates of each 3D group, returning them to their original positions. To complete the first step, the technique compute the estimates by weighted averaging, generating the input image of the second step.

The final estimate is done by grouping similar blocks between the noisy image and the output image from the previously step (basic estimate) into two 3D groups. A 3D transform is applied in both groups and a collaborative Wiener filtering is used to filter the noisy image blocks using the energy spectrum of the basic estimate as the true spectrum, producing estimates of each group. Then, the inverse transform

is applied and the estimates are returned to their original positions. The final output image (see Fig. 2(d)), denoted as f_{10} , is obtained by aggregating all the estimates using weighted average.

Now that the foreground region is completely processed, the noise present in the background region image f_6 must be filtered. For that, we can simply apply another morphological opening operator with the same parameters used before. Done that, the filtered background image f_{11} is obtained and it is possible to see in Fig. 2(e) that the noise was successfully erased.

The last procedure of the noise filtering stage and, consequently, of our proposed method, is to compute the filtered foreground and background regions in order to get the final noise-free output image f_{12} . For that, it is done an addition between f_{10} and f_{11} . Fig. 2(f) shows the final noise-free output image of our proposed method.

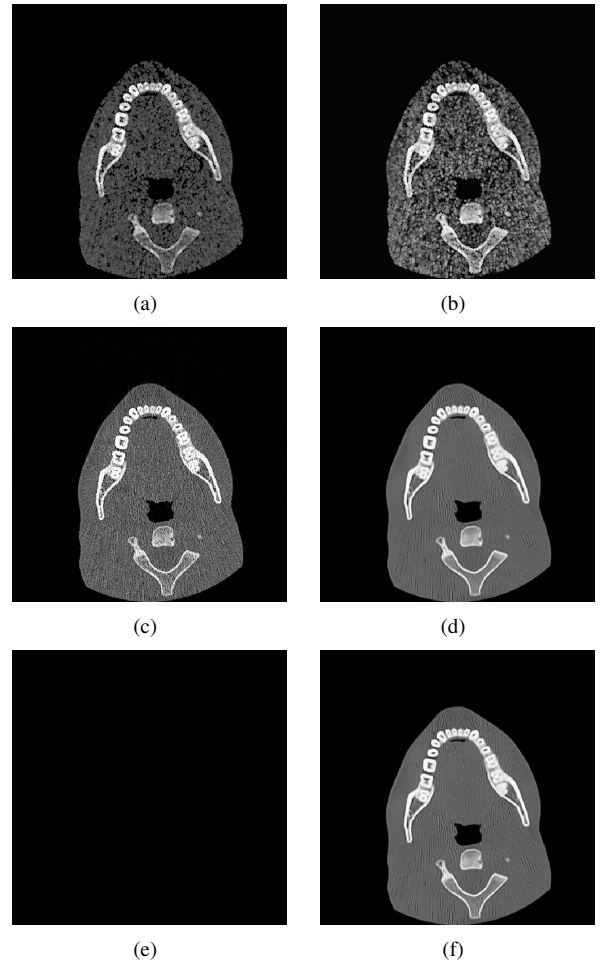


Fig. 2. (a) Resulting image f_7 from opening operator. (b) Resulting image f_8 from CLAHE enhancement. (c) Resulting image f_9 from reconstruction by dilation. (d) Filtered foreground after BM3D. (e) Filtered background. (f) Output image f_{12} of the proposed method.

III. EXPERIMENTAL RESULTS AND VALIDATION

We tested our method on 991 low-dose computed tomography dental images. The images are of size 512x512. Our

experiments were performed using an Intel(R) Core(TM) 2 Duo CPU, clock of 2.00 GHz and 4GB of RAM memory. The algorithms have been implemented in MATLAB R2015a.

The performance of the proposed method is compared with Standard Median Filter (SMF), Wiener, Gaussian, Average, Guided, Bilateral and Bitonic filters, BM3D, AWMF, Visu-Shrink, Anisotropic Diffusion, AMF, PSMF, NAFSMF and OCS filter. For quantitative evaluation, the metrics PSNR, SSIM, MSE and EPI were used. The parameters for each evaluated filter were adjusted to ensure good noise reduction and detail preservation results in both quantitative and visual aspects.

The PSNR (Peak Signal-to-Noise Ratio) metric computes the peak signal-to-noise ratio in decibels between the original image f and the reconstructed image g and can be described as

$$PSNR(f, g) = 10 \log_{10} \left(\frac{255^2}{MSE(f, g)} \right). \quad (4)$$

PSNR values tends to be high when the MSE is low. That said, a higher PSNR value usually means a good image quality [20].

The MSE (Mean-Squared Error) measures the average squared difference between two images. A value closer to zero corresponds good results. The MSE between the original image f and the processed image g , both of sizes $M \times N$, is computed as:

$$MSE(f, g) = \frac{1}{MN} \sum_{i=1}^M \sum_{j=1}^N (f_{ij} - g_{ij})^2. \quad (5)$$

Structural similarity (SSIM) [21] is used to measure the similarity between two images, considering three important factors: loss of correlation, luminance distortion and and contrast distortion [20]. The SSIM is defined as

$$SSIM(f, g) = l(f, g) * c(f, g) * s(f, g) \quad (6)$$

where

$$\begin{aligned} l(f, g) &= \frac{2\mu_f\mu_g + C_1}{\mu_f^2 + \mu_g^2 + C_1} \\ c(f, g) &= \frac{2\sigma_f\sigma_g + C_2}{\sigma_f^2 + \sigma_g^2 + C_2} \\ s(f, g) &= \frac{\sigma_{fg} + C_3}{\sigma_f\sigma_g + C_3} \end{aligned} \quad (7)$$

with $C_1 = (k_1L)^2$, $C_2 = (k_2L)^2$, $C_3 = \frac{C_2}{2}$, $k_1 = 0.01$, $k_2 = 0.02$ and L is the dynamic range of the pixels values. The terms $l(f, g)$ refers to the luminance comparison where μ is the average of f and g ; $c(f, g)$ is the contrast function where σ is the variance of f and g and $s(f, g)$ is the structure comparison function. A value of 0 means no correlation at all between the images and 1 means that the processed image had good structural preservation and is equal to the input image [21].

The EPI (Edge Preservation Index) [22] evaluate the correlation of the edges between two images, which can be expressed as

$$EPI = \frac{\Gamma(\Delta s - \Delta \bar{s}, \Delta \hat{s} - \Delta \bar{\hat{s}})}{\sqrt{\Gamma(\Delta s - \Delta \bar{s}) \cdot \Gamma(\Delta \hat{s} - \Delta \bar{\hat{s}}, \Delta \hat{s} - \Delta \bar{\hat{s}})}} \quad (8)$$

$$\Gamma(s_1, s_2) = \sum_{i, j \in ROI} s_1(i, j) \cdot s_2(i, j)$$

where $\Delta s(i, j)$ and $\Delta \hat{s}(i, j)$ are the highpass filtered version of the region of interest (ROI) in $s(i, j)$ and its transformed version $s_2(i, j)$ obtained with a 3×3 standard approximation of the Laplacian operator. The terms $\Delta \bar{s}$ and $\Delta \bar{\hat{s}}$ are mean values in the ROI of $s(i, j)$ and $s_2(i, j)$, respectively.

The performance results of each filter evaluated above are discussed in Section IV. In addition to quantitative comparisons, shown in Table 1, subjective visual comparisons are also made between images processed by all filters evaluated which are presented in the next section.

TABLE I
PERFORMANCE OF EACH EVALUATED FILTER.

Filters	PSNR	SSIM	MSE	EPI
SMF	21.32	0.33	561.95	0.72
Wiener filter	24.76	0.58	204.31	0.73
Gaussian filter	23.32	0.53	299.64	0.7
Average filter	21.08	0.42	579.03	0.68
Guided filter	21.83	0.48	271.27	0.8
Bilateral filter	23.72	0.57	242.76	0.73
BM3D	25.59	0.63	207.11	0.83
Bitonic filter	21.91	0.48	488.18	0.74
AWMF	22.33	0.38	529.16	0.69
Visu-Shrink	20.74	0.32	673.65	0.51
Anisotropic diffusion	24.02	0.6	288.61	0.79
AMF	21.13	0.49	574.25	0.71
PSMF	21.28	0.45	560.93	0.69
NAFSMF	21.81	0.59	598.32	0.71
OCS	22.95	0.43	466.48	0.75
Proposed	28.78	0.7	177.06	0.91

IV. RESULTS DISCUSSION

Fig. 3 (a) is a noisy low-dose dental computed tomography image taken as input for each simulation. Fig. 3 (b) is the denoised image processed by the SMF, which can be noticed that the noise was well reduced but some small structures and edges got blurred. In Fig. 3 (c) we can notice that the Wiener filter left some noise and created an almost transparent line across the rounded border.

In visual terms, Fig. 3 (d) and Fig. 3 (e) had almost the same performance, although the Average filter had lower PSNR, leading to a less noise reduction efficiency. The image processed by the Guided filter, illustrated in Fig. 3 (f) had its structures and details blurred, as well as the noise present, which was not reduced in a proper way. The bilateral filter (see Fig. 3 (g)) left the image blurred and degraded some small structures and details. The standard BM3D (Block-Matching 3D) filter reduced in part the noise and had the best edge and structure preservation performance among the evaluated filters, proven by its average EPI and SSIM values. The image resulting from this filtering process is illustrated by Fig. 3 (h).

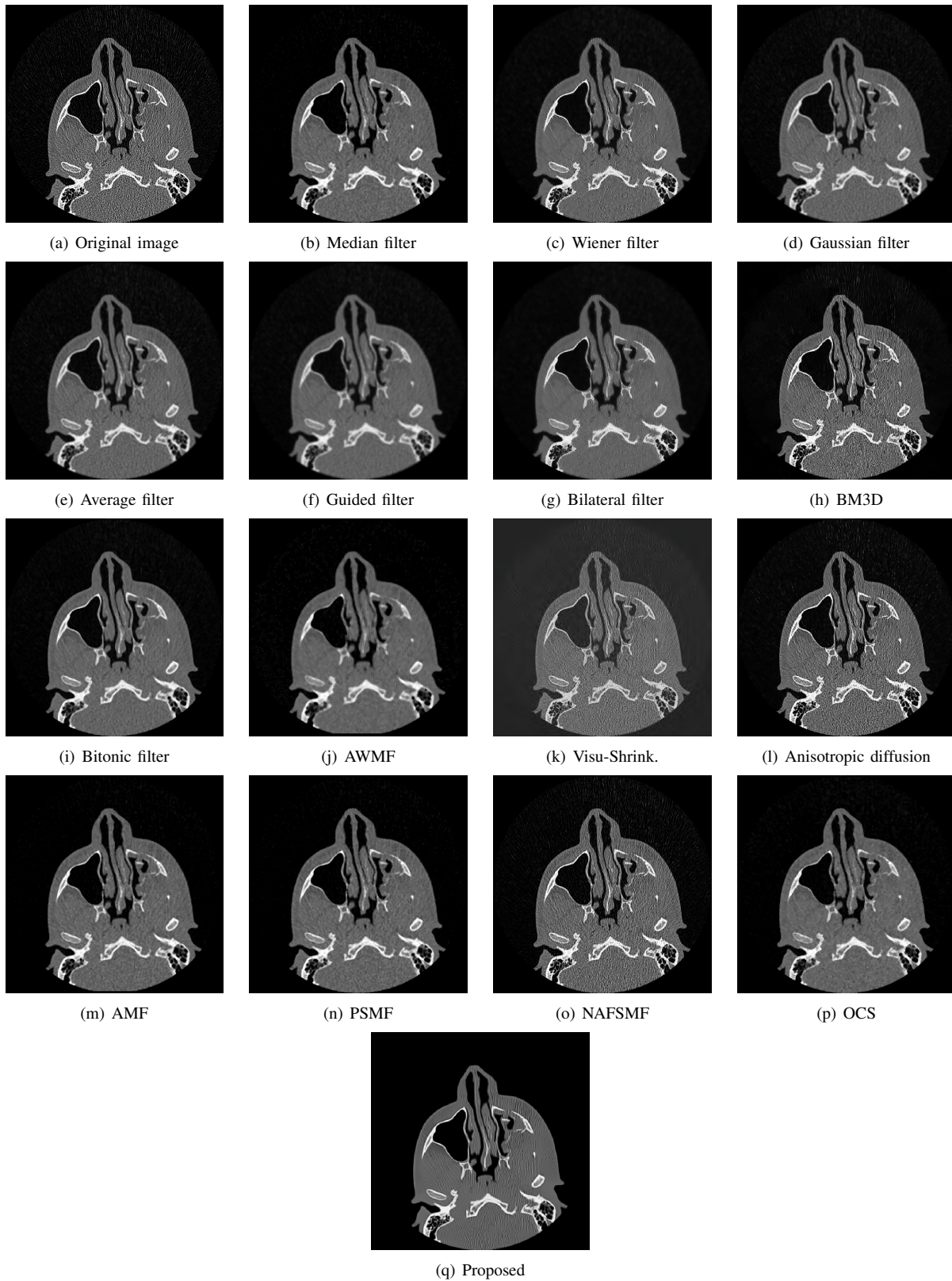


Fig. 3. Noise reduction results of each evaluated filter.

The bitonic filter obtained similar visual results as the Bilateral filter. However, instead of degrading small structures,

the filter left them with a blurry aspect. The AWMF had similar results to the Standard Median Filter, however, the resulting

image (see Fig. 3 (j)) obtained a more expressive blurring aspect in small structures and highlighted some noisy pixels in the image. According to the results shown in Table 1, the Visu-Shrink technique had the worst average results among the compared filters. Also, according to Fig. 3 (k), it had a poor visual performance.

The Anisotropic diffusion technique had a good edge and structure preservation efficiency (see Fig. 3 (l)) with an average EPI and SSIM of 0.79 and 0.6, respectively. On the other hand, the filter was not effective in reducing noise.

The AMF, PSMF and NAFSMF, Figs. 3 (m), (n), (o), respectively, computed close quantitative results in all quality metrics used. Yet, the AMF and PSMF had better visual results when it comes to noise reduction, compared to the NAFSMF.

The morphological Open-Close Sequence (OCS) filter had a good visual noise reduction performance, which can be seen in Fig. 3 (p). Even though its average PSNR value was not the best, the OCS filter showed a good edge preservation, with an average EPI of 0.75. However, small structures and details were poorly preserved, proven by its low average SSIM value of 0.43.

Our proposed method exceeded all the filters evaluated in all the quantitative quality metrics used. In Fig. 3 (q) it is possible to see that our proposed method denoised the image in a satisfactory way, with the best average PSNR value of 28.78. Also, it preserved structures and details better, proved by its average SSIM value of 0.7, had less loss of information, with the lowest average MSE value of 177.06 and obtained the best efficiency in preserving edges, with an average EPI value of 0.91. Compared to the filter which obtained the best quantitative results, the standard BM3D, our method proved to be 12.46%, 11.11%, 14.5% and 9.63% better on PSNR, SSIM, MSE and EPI metrics, respectively.

V. CONCLUSIONS

This paper introduces a method based on mathematical morphology operators and Block-Matching 3D filtering to reduce noise and preserve details in low-dose computed tomography dental images, which is divided into two stages: image segmentation and noise filtering.

The proposed method was tested on 991 images taken from an anonymous database. In simulation experiments, the proposed method is compared with 17 noise reduction filters. The experiments are validated using PSNR, SSIM, MSE and EPI quantitative performance metrics. By comparing the results of each evaluated filter, it is shown that the proposed method performs better than the other filters on noise removing performance, with an average PSNR value of 28.78. Also, the visual results of low-dose CT dental images indicates that the proposed method preserves the image details, such as edges and small structures, proved by its average SSIM and EPI values of 0.7 and 0.91, respectively.

ACKNOWLEDGMENTS

This study was financed in part by the Coordination of Improvement of Higher Level Personnel - Brazil (CAPES) - Finance Code 001.

REFERENCES

- [1] Z. Li, L. Yu, J. D. Trzasko, D. S. Lake, D. J. Blezek, J. G. Fletcher, C. H. McCollough, and A. Manduca, "Adaptive nonlocal means filtering based on local noise level for ct denoising," *Medical physics*, vol. 41, no. 1, 2014.
- [2] I. Pitas and A. N. Venetsanopoulos, "Order statistics in digital image processing," *Proceedings of the IEEE*, vol. 80, no. 12, pp. 1893–1921, 1992.
- [3] J. Feng, M. Ding, and X. Zhang, "Decision-based adaptive morphological filter for fixed-value impulse noise removal," *Optik-International Journal for Light and Electron Optics*, vol. 125, no. 16, pp. 4288–4294, 2014.
- [4] F. Bergholm, "Edge focusing," *IEEE Transactions on Pattern Analysis and Machine Intelligence*, no. 6, pp. 726–741, 1987.
- [5] C. Tomasi and R. Manduchi, "Bilateral filtering for gray and color images," in *Computer Vision, 1998. Sixth International Conference on*. IEEE, 1998, pp. 839–846.
- [6] G. Trecece, "The bitonic filter: linear filtering in an edge-preserving morphological framework," *IEEE Transactions on Image Processing*, vol. 25, no. 11, pp. 5199–5211, 2016.
- [7] K. He, J. Sun, and X. Tang, "Guided image filtering," *IEEE transactions on pattern analysis & machine intelligence*, no. 6, pp. 1397–1409, 2013.
- [8] K. Dabov, A. Foi, V. Katkovnik, and K. Egiazarian, "Image denoising by sparse 3-d transform-domain collaborative filtering," *IEEE Transactions on image processing*, vol. 16, no. 8, pp. 2080–2095, 2007.
- [9] D. L. Donoho and I. M. Johnstone, "Adapting to unknown smoothness via wavelet shrinkage," *Journal of the american statistical association*, vol. 90, no. 432, pp. 1200–1224, 1995.
- [10] T. Loupas, W. McDicken, and P. L. Allan, "An adaptive weighted median filter for speckle suppression in medical ultrasonic images," *IEEE transactions on Circuits and Systems*, vol. 36, no. 1, pp. 129–135, 1989.
- [11] Z. Wang and D. Zhang, "Progressive switching median filter for the removal of impulse noise from highly corrupted images," *IEEE Transactions on Circuits and Systems II: Analog and Digital Signal Processing*, vol. 46, no. 1, pp. 78–80, 1999.
- [12] K. K. V. Toh and N. A. M. Isa, "Noise adaptive fuzzy switching median filter for salt-and-pepper noise reduction," *IEEE signal processing letters*, vol. 17, no. 3, pp. 281–284, 2010.
- [13] K. Vasanth, T. Manjunath, and S. N. Raj, "A decision based unsymmetrical trimmed modified winsorized mean filter for the removal of high density salt and pepper noise in images and videos," *Procedia Computer Science*, vol. 54, pp. 595–604, 2015.
- [14] U. Erkan and L. Gökrem, "A new method based on pixel density in salt and pepper noise removal," *Turkish Journal of Electrical Engineering & Computer Sciences*, vol. 26, no. 1, pp. 162–171, 2018.
- [15] D. Ze-Feng, Y. Zhou-Ping, and X. You-Lun, "High probability impulse noise-removing algorithm based on mathematical morphology," *IEEE signal processing Letters*, vol. 14, no. 1, pp. 31–34, 2007.
- [16] C. Solomon and T. Breckon, *Fundamentos de processamento digital de imagens: uma abordagem prática com exemplos em Matlab*. Grupo Gen-LTC, 2000.
- [17] S. Masood, M. Sharif, A. Masood, M. Yasmin, and M. Raza, "A survey on medical image segmentation," *Current Medical Imaging Reviews*, vol. 11, no. 1, pp. 3–14, 2015.
- [18] N. Otsu, "A threshold selection method from gray-level histograms," *IEEE transactions on systems, man, and cybernetics*, vol. 9, no. 1, pp. 62–66, 1979.
- [19] A. M. Reza, "Realization of the contrast limited adaptive histogram equalization (clahe) for real-time image enhancement," *Journal of VLSI signal processing systems for signal, image and video technology*, vol. 38, no. 1, pp. 35–44, 2004.
- [20] A. Hore and D. Ziou, "Image quality metrics: Psnr vs. ssim," *20th International Conference on Pattern Recognition*, pp. 2366–2369, 2010.
- [21] Z. Wang, A. C. Bovik, H. R. Sheikh, and E. P. Simoncelli, "Image quality assessment: from error visibility to structural similarity," *IEEE transactions on image processing*, vol. 13, no. 2, pp. 600–612, 2004.
- [22] F. Sattar, L. Floreby, G. Salomonsson, and B. Lovstrom, "Image enhancement based on a nonlinear multiscale method," *IEEE transactions on image processing*, vol. 6, no. 6, pp. 888–895, 1997.